Saitta, E. T., Fletcher, I., Martin, P. G., Pittman, M., Kaye, T. G., True, L. D., ... Vinther, J. (2018). Preservation of feather fibers from the Late Cretaceous dinosaur Shuvuuia deserti raises concern about immunohistochemical analyses on fossils. *Organic Geochemistry*, *125*, 142-151. https://doi.org/10.1016/j.orggeochem.2018.09.008

Accepted Manuscript

Preservation of feather fibers from the Late Cretaceous dinosaur *Shuvuuia deserti* raises concern about immunohistochemical analyses on fossils

Evan T. Saitta, Ian Fletcher, Peter Martin, Michael Pittman, Thomas G. Kaye, Lawrence D. True, Mark A. Norell, Geoffrey D. Abbott, Roger E. Summons, Kirsty Penkman, Jakob Vinther

PII: S0146-6380(18)30219-5
DOI: https://doi.org/10.1016/j.orggeochem.2018.09.008
Reference: OG 3786

To appear in: *Organic Geochemistry*

Received Date: 19 June 2018
Revised Date: 7 September 2018
Accepted Date: 9 September 2018

Please cite this article as: Saitta, E.T., Fletcher, I., Martin, P., Pittman, M., Kaye, T.G., True, L.D., Norell, M.A., Abbott, G.D., Summons, R.E., Penkman, K., Vinther, J., Preservation of feather fibers from the Late Cretaceous dinosaur *Shuvuuia deserti* raises concern about immunohistochemical analyses on fossils, *Organic Geochemistry* (2018), doi: https://doi.org/10.1016/j.orggeochem.2018.09.008

Preservation of feather fibers from the Late Cretaceous dinosaur *Shuvuuia deserti* raises concern about immunohistochemical analyses on fossils

Evan T. Saitta[a,1,*], Ian Fletcher[b], Peter Martin[c], Michael Pittman[d], Thomas G. Kaye[e], Lawrence D. True[f], Mark A. Norell[g], Geoffrey D. Abbott[h], Roger E. Summons[i], Kirsty Penkman[j], Jakob Vinther[a,k]

[a] *School of Earth Sciences, University of Bristol, Bristol BS8 1RJ, UK*

[b] *School of Natural and Environmental Sciences, Drummond Building, Newcastle University, Newcastle upon Tyne NE1 7RU, UK*

[c] *School of Physics, University of Bristol, Bristol BS8 1TL, UK*

[d] *Vertebrate Palaeontology Laboratory, Department of Earth Sciences, The University of Hong Kong, Pokfulam, Hong Kong, China*

[e] *Foundation for Scientific Advancement, Sierra Vista, AZ 85650, USA*

[f] *Department of Pathology, University of Washington, Seattle, WA 98195, USA*

[g] *Division of Paleontology, American Museum of Natural History, New York, NY 10024, USA*

[h] *School of Natural and Environmental Sciences, Drummond Building, Newcastle University, Newcastle upon Tyne NE1 7RU, UK*

[i] *Department of Earth, Atmospheric and Planetary Sciences, Massachusetts Institute of Technology, Cambridge, MA 02139, USA*

[j] *Department of Chemistry, University of York, York YO10 5DD, UK*

[k] *School of Biological Sciences, University of Bristol, Bristol BS8 1TQ, UK*

[1] Present address: Integrative Research Center, Section of Earth Sciences, Field Museum of Natural History, Chicago, Illinois 60605, USA

* Corresponding author at: Integrative Research Center, Section of Earth Sciences, Field Museum of Natural History, Chicago, Illinois 60605, USA.
E-mail address: evansaitta@gmail.com (E. T. Saitta).

Declarations of interest: None

ABSTRACT

White fibers from a Late Cretaceous dinosaur *Shuvuuia deserti* stained positive for β-keratin antibodies in a 1999 paper, followed by many similar immunological claims for Mesozoic protein in bones and integument. Antibodies recognize protein epitopes derived from its tertiary and quaternary structure, so such results would suggest long polypeptide preservation allowing for sequencing with palaeobiological implications. However, proteins are relatively unstable biomacromolecules that readily hydrolyze and amino acids exhibit predictable instability under diagenetic heat and pressure. Furthermore, antibodies can yield false positives. We reanalyzed a *Shuvuuia* fiber using focused ion beam scanning electron microscopy, energy-dispersive X-ray spectroscopy, time-of-flight secondary ion mass spectrometry, and laser-stimulated fluorescence imaging, finding it to be inorganic and composed mainly of calcium phosphate. Our findings are inconsistent with any protein or other original organic substance preservation in the *Shuvuuia* fiber, suggesting that immunohistochemistry may be inappropriate for analyzing fossils due to issues with false positives and a lack of controls.

Keywords: fossils; feathers; antibodies; keratin; calcium phosphate; protein

1. Introduction

Organic 'soft tissue' preservation in Mesozoic fossils has been reported for over three decades (De Jong et al., 1974; Gurley et al., 1991; Schweitzer et al., 2005, 2007, 2009; Asara et al., 2007; Bertazzo et al., 2015; Moyer et al., 2016a, 2016b; Pan et al., 2016). The identification of organically preserved, tens-of-millions-of-years-old proteins, cells, and tissues would be groundbreaking, with potential for studying molecular evolution through geologic time and illuminating extinct animal physiologies. Early work reported β-keratin in bird and non-avian dinosaur integumentary structures (Schweitzer et al., 1999a, 1999b), such as IGM 100/977 (Mongolian Institute of Geology, Ulaan Bataar, Mongolia), a specimen of the small, bipedal Late Cretaceous alvarezsaurid theropod dinosaur *Shuvuuia deserti* from the Mongolian Djadochta Formation with multiple thin fibers associated with the skeleton interpreted as primitive feathers (Schweitzer et al., 1999b).

However, proteins are unstable over deep geologic time (Kriausakul and Mitterer, 1978; Armstrong et al., 1983; Lowenstein,1985; Mitterer, 1993; Bada, 1998; Briggs and Summons, 2014; Saitta et al., 2017). Partially intact proteins persist for 3.4 Ma in exceptionally cold environments (Rybczynski et al., 2013). Biomineralized calcite crystals can act as closed systems with respect to intracrystalline biomolecules although degradation of these biomolecules still occurs (Curry et al., 1991) (e.g., in a survey of New Zealand brachiopod shells, immunological signals correlated with

peptide hydrolysis but were lost by 2 Ma (Walton, 1998; Collins et al., 2003)). The oldest, uncontested, low-latitude peptide sequence is a short, acidic peptide found within ~3.8 Ma ratite eggshells (Demarchi et al., 2016). The sequence was a disordered aspartic acid-rich region of the eggshell protein struthiocalcin. Its survival is exceptional since carbonate-bound proteins degrade rapidly and predictably (Curry et al., 1991; Walton, 1998; Collins et al., 2003), explaining their utility in amino acid racemization dating, and the surviving region was independently predicted by molecular simulation from four candidate binding regions. The disordered and otherwise unstable sequence adopted a stable configuration when bound to the calcite which in effect 'froze' the peptide to the surface, dropping the local system temperature by ~30 K, as described by Demarchi et al. (2016). While short peptide sequences are relatively common from younger Pleistocene sub-fossils (Orlando et al., 2013), these are over two orders of magnitude younger than purported antibody-based Mesozoic peptides.

Antibodies are immune system proteins with unique molecular structures that can bind to distinct epitopes on antigens, which are exogenous substances triggering an immune response, such as pathogens. Antibody-antigen binding specificity has been co-opted for research and medical purposes, but false positives are common and of concern for any experiment (True, 2008). Binding specificity is the basis of immunohistochemical experiments performed on *Shuvuuia* fibers and other fossils reporting the presence of β-keratin (Schweitzer et al., 1999a, 1999b;

Moyer et al., 2016a, 2016b). A true positive would suggest long, likely intact, peptide sequence preservation with higher-order protein folding, given the conformation-based nature of antibody-antigen binding specificity (Laver et al., 1990). Beyond the unlikelihood of Mesozoic protein folding preservation, another issue with these immunochemistry studies is that molecular dating of the evolution of keratin proteins indicates that modern feather β-keratins diverged ~143 Ma, meaning that the feathers of non-avian dinosaurs such as *Shuvuuia* might not have been composed of the same family of avian β-keratins as that of modern feathers (Greenwold and Sawyer, 2011). This would mean that modern feather keratin is the wrong antigen to raise antibodies against for experiments on *Shuvuuia* keratin.

The possibility that these results represent false positives is investigated here. Accordingly, we analyzed *Shuvuuia* fiber composition by examining another fiber from IGM 100/977 (see Schweitzer et al., 1999b; Moyer et al., 2016a for immunochemistry result on fibers from this same specimen). A small piece of matrix containing the fiber studied here was originally removed from the specimen in 2009 by Amy Davidson who originally prepared the specimen, stored at room temperature within paper towel wrapping, and analyzed from 2016 onwards (potentially increasing the likelihood of detecting proteinaceous signatures in the form of contamination). The original report of β-keratin in IGM 100/977 was published in 1999 (Schweitzer et al., 1999b), and the fiber used in this study received no further preparation prior to our study. If the fibers indeed

contain endogenous keratin, then the ~17 years between studies is unlikely to result in much degradation, considering their putative persistence since the Late Cretaceous and withstanding diagenesis, environmental moisture in the surface or subsurface, climatic and geothermal high temperatures, and weathering. Therefore, although atmospheric exposure might be argued to impose different degradation stresses on the fossil (e.g., increased oxidation or decay from newly introduced aerobic microbes) than do burial and diagenesis that could result in a loss of original protein over ~17 years, we consider this to be unlikely.

If the fiber is indeed composed of keratin, then it should contain signatures consistent with proteins and organic material more generally. Therefore, this study examines the basic structure and chemistry of the fiber. We analyzed the fiber using light microscopy, laser-stimulated fluorescence (LSF) imaging (Kaye et al., 2015; Wang et al., 2017), time-of-flight secondary ion mass spectrometry (TOF-SIMS), scanning electron microscopy (SEM), and energy-dispersive X-ray spectroscopy (EDS). The untreated fiber and surrounding sediment matrix underwent light microscopy and LSF imaging and a fragment of fiber and matrix underwent TOF-SIMS. After discovering that the fiber and matrix were covered by cyanoacrylate consolidant, a focused ion beam (FIB) trench of the fiber fragment was analyzed under SEM and EDS. Finally, the fragment of the fiber and surrounding sediment matrix were resin-embedded, polished, and the cross-section was analyzed with SEM, EDS, and TOF-SIMS.

2. Material and methods

2.1. Light microscopy and LSF

LSF images were collected using a modified version of the protocol of Kaye et al. (2015). The untreated fiber and surrounding sediment matrix was illuminated with a 405 nm, 500 mw violet laser diode and imaged with a Leica DFC425 C digital camera under magnification from a Leica M205 C stereomicroscope. An appropriate long pass blocking filter was fitted to the objective of the stereoscope to prevent image saturation by the laser. The laser diode was defocused to project a beam cone that evenly lit the specimen during the photo's time exposure in a dark room. The images were post-processed in Photoshop CC 2016 for sharpness, color balance, and saturation.

2.2. SEM and EDS

Following light microscopy and LSF, a fragmented portion of the fiber and surrounding sediment matrix was sputter-coated with a 50 nm thick layer of gold using an Edwards ScanCoat system to prevent specimen-induced charging and difficulties with imaging/cutting. FIB preparation was performed with a FEI Helios NanoLab 600 dual FIB-SEM system. Before the cross-section was produced (approximately 40 µm × 20 µm × 20 µm), a protective strip of platinum was deposited over the region bordering the cut to prevent against any potential ion-beam damage to the sample surface.

Milling was conducted at 30 kV with progressively lower beam currents (6.0 nA to 0.9 nA) to produce an artefact-free surface.

The same fragment of fiber and surrounding sediment matrix was later embedded in EpoThin 2 epoxy resin and polished using silicon carbide paper to reveal a cross-section of the fiber. SEM and EDS analysis of the FIB-trenched, and subsequently, the resin-embedded polished sample was conducted within a Zeiss SIGMA-HD VP scanning electron microscope with associated EDS instrumentation from EDAX Ltd. The EDS system consisted of an Octane Plus Si-drift detector alongside TEAM control and analysis software.

Spot compositional analysis was performed on the samples at 15 kV and 1.7 nA electron beam current for a duration of 100 s per point before progressing onto the next user-defined point. Elemental mapping of the ion-beam cut surface was conducted using the same instrument to visually identify regions of compositional similarity and variation. All EDS analyses were taken in cross-sectional or top-down view in order to mitigate artefacts deriving from the orientation angle of the detector relative to one axis of the specimen.

2.3. TOF-SIMS

The fiber and surrounding sediment matrix underwent TOF-SIMS untreated and, later, resin-embedded polished. The samples were mounted

directly onto a sample holder using double-sided carbon tape or clean stainless steel screws and clips as appropriate.

Static SIMS analyses were carried out using an ION-TOF 'TOF-SIMS IV – 200' instrument (ION-TOF GmbH, Münster, Germany) of single-stage reflectron design (Schwieters et al., 1991). Positive and negative ion spectra and images were obtained using a Bi_3^+ focused liquid metal ion gun at 25 keV energy, incident at 45° to the surface normal and operated in 'bunched' mode for high mass resolution. This mode used 20 ns wide ion pulses at 10 kHz repetition rate. Charge compensation was effected by low-energy (~20 eV) electrons provided by a flood gun. The total ion dose density was less than 1×10^{16} ions m^{-2}. The topography of the sample surface and the ion gun mode of operation limited the mass resolution in this work to approximately m/Dm = 2000. The spatial resolution was limited by the primary ion beam diameter to ~4 µm.

Initial analysis of untreated sample: Positive and negative ion static SIMS spectra and images were recorded from the outermost ~1 nm of the sample surface at room temperature. Raw data containing the secondary ions recorded at each pixel was acquired with a 256 pixel × 256 pixel raster and a field of view of 256 µm × 256 µm.

Subsequent analysis of resin-embedded polished sample: The area to be analyzed was sputtered using the Bi_3^+ ion beam in 'continuous' or 'DC' mode for 240 s in an attempt to remove any contamination from the polishing process. The ion beam current was 0.5 nA and the ion dose density

was less than 1×10^{19} ions m^{-2}. Positive and negative ion static SIMS spectra and images were recorded from the outermost ~ 1 nm of the sample surface at room temperature. Raw data containing the secondary ions recorded at each pixel was acquired with a 256 pixel × 256 pixel raster and a field of view of 500 μm × 500 μm.

Images were regenerated from selected peaks in the raw datasets following a full recalibration of the mass scale using the 'Ionspec' and 'Ionimage' software from ION-TOF GmbH. The images are presented un-normalized with a linear intensity scale and after Poisson correction for the detector dead-time effects. The images are shown in thermal scale which runs from black through red, orange, and yellow to white with increasing signal intensity.

Using the software to select pixels in regions of interest from the total ion image allowed spectra of the fiber and matrix regions in the sample to be generated from the raw data collected by the ION-TOF 'TOF-SIMS IV – 200'.

3. Results

3.1. Light microscopy and LSF

The fiber resides within loosely consolidated, predominantly sand-sized quartz grains (Fig. 1A–C). The fiber is a pale, white cylinder with unidirectional tapering and occasional breakages. White residues similar in color and texture to the fiber also appear in adjacent sediment near the

fiber. Some fiber segments are missing through breakage (as evidenced by the fact that the specimen has multiple fibers preserved that vary in continuity and consistent with the loosely consolidated nature of the sediment) and others deflect around sediment grains. The fiber is 7.7 mm in linear length and ranges in width from 0.25 mm basally to 0.03 mm apically. LSF reveals that the fiber fluoresces a different color to the surrounding sediment grains (Fig. 1D).

3.2. TOF-SIMS

In the untreated sample, both the fiber and sediment grains have strong CN^- (m/z = –26) peaks as well as strong peaks at m/z = –112 consistent with $C_5H_6NO_2^-$ (Supplementary Figs. S135–S136). The sediment grains and fiber have very similar spectra over the entire m/z range examined, consisting largely of organic secondary ions (Supplementary Figs. S137–S140).

In the resin-embedded polished sample (Fig. 2A), secondary ions such as Ca^+, CaO_x^+, $CaPO_x^+$, and PO_x^- were strongly localized to the fiber (Fig. 2B–F). Secondary ions such as Mg^+, Fe^+, K^+, Al^+, Na^+, Si^+, Si^-, SiO_x^-, and Cl^- were present in the sediment grains at elevated levels compared to the fiber, although low levels of Na^+, relative to the grains, show some non-specific localization to the fiber as well (Fig. 2G–O). Secondary ions related to epoxy (both positive and negative) and cyanoacrylate (negative) residues appear on the grains, fiber, and embedding resin (Fig. 2P–R). Of the secondary ions

examined that can potentially relate to amino acids such as those identified by Hedberg et al. (2012) (Fig. 2S–JJ), total N^+ (Fig. 2KK), and S^- (Fig. 2LL), none showed preferential localization to the fiber, and most were detected at low levels broadly across the grains, fibers, and embedding resin, while CN^- strongly localized to the embedding resin (Fig. 2S–MM). Furthermore, peaks at m/z = 76.02 that could possibly come from $C_2H_6SN^+$ are not strongly present in the fiber and are more expressed in the sediment grains and embedding resin.

3.3. SEM and EDS

To reveal the internal composition in a minimally intrusive fashion, a trench was milled using FIB. SEM reveals the fiber's corrugated surface and platy core textures (Fig. 1E), although the potential for 'curtaining' artifacts from FIB should be kept in mind. EDS up the FIB section from the more interior region onto the uncut surface shows consistent elemental makeup with strong Ca, C, Si, Al, O, and P peaks (Supplementary Figs. S1–S22, Supplementary Tables S1–S7). Other small peaks detected include Fe, Mg, and Na. S peaks are weak in all spectra. Ga peaks are a result of implantation from FIB. Top-down elemental maps (i.e., trench viewed perpendicular to the fiber surface as opposed to viewing the wall of the FIB trench which is perpendicular to the fiber surface) show potential preferential localization of C to the uncut surface (Supplementary Figs. S23–S41, Supplementary Tables S8–S12).

The resin-embedded polished sample shows a similar, yet stronger signal, without topographic artifacts inevitably present in the EDS of the FIB trench. The platy texture of the fiber core still seems apparent (Fig. 3A). Ca and P are strongly localized in the fiber, and although Si, Al, and O are also present, they are more prevalent in adjacent sediment grains. S is weakly expressed in the fiber and sediment. Mg is present in small amounts in the fiber. Na is more prevalent in the sediment than the fiber, while Fe mostly appears in the space between the fiber and sediment grains (Fig. 3B–I). No substantial C was detected (Fig. 3J).

4. Discussion

The analyses performed here reveal four key aspects of the fiber's chemistry: it is covered in cyanoacrylate, it is largely calcium phosphate, it lacks chemical signatures consistent with protein, and it likely has clay mineral infiltration within the possibly endogenous calcium phosphate.

TOF-SIMS data suggest that the fiber and surrounding sediment are encapsulated in ethyl-cyanoacrylate polymer as indicated by the presence of $C_5H_6NO_2^-$ secondary ions (Supplementary Figs. S135–S140), deriving from the consolidant used in the original preparation of the fossil to stabilize the specimen prior to the Schweitzer et al. (1999b) study (Krazy Glue™ 201 ethyl-cyanoacrylate, white cap, low viscosity, Borden Inc., purchased in 1994, and used in addition to Butvar B-76 [polyvinyl butyral]; Amy Davidson personal communication). The presence of cyanoacrylate first

became apparent when analyzing the untreated sample with TOF-SIMS, prior to embedding in resin and polishing. Cyanoacrylate was detected strongly in the untreated sample, but was detected as a diffuse pattern (along with epoxy embedding resin; Fig. 2P and Q) across the entire surface of the polished sample likely due to grinding (Fig. 2R). EDS detected surface consolidant as C (Supplementary Figs. S1–S41, Supplementary Tables S1–S12).

EDS of the fiber core revealed Ca, P, and O, consistent with calcium phosphate (Fig. 3B–D and J). TOF-SIMS corroborated this composition with preferential localization of Ca^+, CaO_x^+, $CaPO_x^+$, and PO_x^- to the fiber, while the lack of Ca^- was consistent with Ca derived from the cation of $CaPO_4$ (Fig. 2B–F). TOF-SIMS carried out by Schweitzer et al. (1999b) also detected Ca^+ and CaO_2^+ in *Shuvuuia* (IGM 100/977) fibers.

Very little S was observed in the fiber through EDS, which would have been present in stable disulfide bonds of keratin protein in vivo (Goddard and Michaelis, 1934); no significant N was observed, strongly suggesting the absence of protein since N is incorporated into peptide bonds (Fig. 3I and J). TOF-SIMS showed a lack of preferential localization of any of the examined potential amino acid fragment ions from Hedberg et al. (2012) (work which relates secondary ions to the particular amino acid they can derive from), total N^+, or S^- to the fiber (Fig. 2S–MM). Relatively uniform, low-intensity distributions across the polished section of some of these fragment ions suggests that they largely came from spreading of

applied consolidant residues during grinding. Given the lack of S^-, peaks at m/z = 76.02 are likely due to $C_5H_2N^+$ (m/z = 76.018) and/or $C_2H_4O_3^+$ (m/z = 76.016) rather than $C_2H_6SN^+$ deriving from the cysteine found abundantly in keratin and responsible for forming disulfide bridges. Regardless, m/z = 76.02 peaks do not strongly appear in the fiber, but rather in the sediment grains and embedding resin (Fig. 2CC). What little S is present in the fiber could potentially be in an inorganic form such as pyrite, which is commonly found in fossils. Some of the S atoms themselves, however, could have originally been released from keratin breakdown products. Previously-published, positive-ion TOF-SIMS data of *Shuvuuia* (IGM 100/977) fibers revealed the presence of various organic secondary ions, interpreted as deriving from endogenous keratin amino acids (Schweitzer et al., 1999b), which are likely derived from either non-amino acid molecules or from amino acid contamination, possibly bound with cyanoacrylate. A further issue with the TOF-SIMS analysis of Schweitzer et al. (1999b) is that it did not present the results from the sediment matrix control in the main text that might elucidate localization patterns, or lack thereof, of these organic secondary ions.

Potential clay presence in the fiber suggested by EDS as Si, Al, and O (Fig. 3D–F and J) is consistent with SEM observations of a platy texture within the FIB trench and resin-embedded polished sample, keeping in mind the potential for FIB artifacts (Fig. 1E). Furthermore, the observed ultrastructural texture and internal structure do not match descriptions of

those from modern feathers (Davies 1970; Lucas and Stettenheim, 1972). TOF-SIMS did not reveal clay markers in the fiber as EDS did, perhaps due to lower resolution mapping (e.g., Mg^+, Fe^+, Al^+, Na^+, Si^+, Si^-, SiO_x^-), but did show non-specific Na^+ presence in the fiber at lower levels than the sediment grains (Fig. 3G–O). Ultimately, calcium phosphate dominance in the fiber is consistent with the differing fiber autofluorescence to the surrounding silicate-dominated sediment matrix during LSF (Fig. 1D). Similar to the data here, Schweitzer et al. (1999b) detected Na^+, Al^+, and Si^+ in *Shuvuuia* (IGM 100/977) fibers using TOF-SIMS.

4.1. Calcium phosphate preservation of fossil keratinous structures: updating the taphonomic model

Endogenous organic carbon in *Shuvuuia* fibers cannot be confirmed, especially in light of the detection of applied cyanoacrylate. Their white coloration is consistent with a lack of organic carbon. Similarly, fossil bone from the Djadochta Formation is also white, again consistent with organic loss.

Keratinous structures (i.e., the anatomical structure/tissue originally containing keratin protein in vivo) commonly fossilize as white, fluorescing material, such as claw sheaths preserved in the Djadochta Formation (Moyer et al., 2016b) and other Mesozoic localities (Martin et al., 1998; Schweitzer et al., 1999a). For example, *Psittacosaurus* integument appears

to preserve as fluorescent calcium phosphate with associated fossil melanin (Mayr et al., 2016; Vinther et al., 2016).

Moyer et al. (2016b) ran EDS on white claw sheaths from the oviraptorid theropod dinosaur *Citipati*, similarly preserved from the same formation as *Shuvuuia* and also claimed to contain keratin protein based on immunohistochemistry. Their study similarly revealed the *Citipati* claw sheaths to be predominantly composed of Ca and O, with P also present, indicating preservation as calcium phosphate. EDS on *Citipati* claw sheaths did not reveal S, suggesting that phosphatic preservation of keratinous tissues need not contain S. Platy textures found in *Citipati* claw sheaths similar to those observed here in the *Shuvuuia* fiber were interpreted as keratin by Moyer et al. (2016b), but our study suggests that such textures are likely not indicative of protein preservation. EDS on *Citipati* claw sheaths similarly revealed the presence of Si, Al, and Mg (Moyer et al., 2016b), consistent with clay mineral infiltration.

Most research into fossil feathers focuses on organically preserved specimens, as in the field of paleo-color reconstruction (Vinther, 2015), probably partly related to the richness of exceptional carbonaceous fossils from China (Norell and Xu, 2005) and similar Lagerstätten. However, calcium and phosphorus are known to be concentrated in *Archaeopteryx* feather rachi (Bergmann et al., 2010) and an isolated Liaoning feather (Benton et al., 2008). North American Mesozoic fossil discoveries in particular, unlike those from Konservat-Lagerstätten with extensive

carbonaceous preservation as in some Chinese deposits, provide an example of alternative preservational modes for keratinous structures. Contrary to finer-grained, anoxic depositional environments that retain and preserve organic molecules like fossil melanin (Fürsich et al., 2007), North American Mesozoic keratinous fossils are often from coarser-grained, oxidized depositional environments adverse to organic retention and preservation (Parry et al., 2018). Instead, Mesozoic keratinous fossils in North America are often preserved as simple skin impressions in the sediment (Bell, 2012) – possibly explaining why large Chinese tyrannosaurs are preserved with carbonaceous fossil feathers (Xu et al., 2012), while large North American tyrannosaurs only preserve scale impressions (Bell et al., 2017).

In some cases, however, North American fossil keratinous structures appear to preserve in a manner consistent with phosphatized sheaths. Ungual and beak sheaths on hadrosaurs (Murphy et al., 2006) and osteoderm sheaths in stegosaurs (Christiansen and Tschopp 2010) are potentially some examples of phosphatized keratinous fossils, deserving of further chemical analyses. The North American ankylosaur *Borealopelta* has osteoderm sheaths with preserved melanin and calcium phosphate, although this rare specimen was found in an exceptional carbonate concretion formed under euxinic conditions (Brown et al., 2017). As for filamentous keratin, Late Miocene phosphatized baleen has been reported from South America (Gioncada et al., 2016). Regarding this *Shuvuuia* specimen, the loosely consolidated, sand-sized quartz grains of the matrix

would not be expected to retain organics well due to the potential leaching of breakdown products through the relatively large pore size or through relatively greater exposure to adverse conditions such as oxidation, so phosphate-dominated preservation of fibers is not unexpected.

A phosphatic preservational mode of fossil keratinous structures is unsurprising since many different keratinous tissues are hardened via calcium phosphate deposition in vivo to varying degrees. For example, calcium phosphate has been measured or detected in fresh/modern claw, horn, beak, and hoof sheaths, nails, baleen, hair, quills, whiskers, and feathers, especially feather calami (Blakey et al., 1963; Pautard, 1963, 1964, 1970; Blakey and Lockwood 1968; Lucas and Stettenheim 1972; Szewciw et al., 2010). Calcification of keratinous structures appears to change their material properties of the integumentary structure, positively correlating with hardness and presumably related to the biological function of the structure (Baggott et al., 1988; Bonser, 1996; Szewciw et al., 2010).

Fossil keratinous tissues likely undergo significant volume loss due to protein degradation, with resistant calcium phosphate and pigments remaining (Saitta et al., 2017). Volume loss would allow for clay minerals to precipitate into the fossil as evidenced by clay signatures in *Shuvuuia* fibers and *Citipati* claw sheaths (Moyer et al., 2016b). Future work should be conducted to determine to what degree phosphatic preservation of keratinous structures represents endogenous calcium phosphate with subsequent infilling of other materials (e.g., clay minerals), or if endogenous

calcium phosphate can act as a nucleus for additional, secondary calcium or phosphate precipitation during fossilization. If the former, then phosphatized keratinous structure fossils could provide important paleobiological data regarding the shape, size, and degree and distribution of calcification of integumentary structures in vivo.

It might be argued that the keratin protein could be phosphatized through authigenic mineralization as a result of decay, as is the case with fossil muscle tissue (Briggs et al., 1993; Briggs and Wilby, 1996; Briggs, 2003; Parry et al., 2015). However, invoking authigenic mineralization as an explanation for keratinous structure fossilization is unnecessary since they can contain calcium phosphate endogenously. Our taphonomic model is consistent with the fact that phosphatic keratinous tissue fossils are often structures expected to be hardened in vivo (e.g., claw, osteoderm, and beak sheaths). Furthermore, authigenically phosphatized tissue tends to preserve small structural details with high fidelity, which does not appear to be the case for some fossil keratinous structures such as the *Shuvuuia* fibers.

IGM 100/977 fibers likely derive from feathers rather than the taphonomic environment based on their distinct, tapering morphology as well as their distribution and orientation around the bones. Furthermore, the structures likely do not represent tissue types other than integumentary structures, such as dermal collagen or muscle. The claim that dermal collagen has been found fossilized as fibers has been heavily refuted (Smithwick et al., 2017), and although muscle tissue can phosphatize via

authigenic mineralization (Briggs et al., 1993; Briggs and Wilby, 1996; Briggs, 2003; Parry et al., 2015), the sparse distribution of the *Shuvuuia* fibers and their orientation around the bones is inconsistent with phosphatized masses of muscle. Given that the fibers are calcium phosphate, *Shuvuuia* feathers were likely hardened in vivo. As rachi might be expected to be preferentially calcified (Pautard, 1964; Benton et al., 2008; Bergmann et al., 2010; also see Supplementary Fig. S141 for an LSF image of a modern feather rachis with prominent fluorescence consistent with calcification), *Shuvuuia* feathers could have consisted of a well-developed rachis with less calcified barbs being unpreserved in this specimen, except possibly for some calcium phosphate residues in the matrix. Such an interpretation is consistent with alvarezsaurid phylogenetic position, since closely related maniraptoriformes are known to have pinnate feathers (Cau et al., 2015) more closely resembling the morphology of many modern feathers (Lucas and Stettenheim, 1972) than to simple monofilaments. In this case, former interpretations of morphologically simple monofilaments typically assumed for alvarezsaurids (Xu et al., 2014) may be taphonomically biased. Therefore, a more complex feather morphology is potentially a better supported hypothesis than simple, calcified monofilaments such as those in *Psittacosaurus*. Unlike the short fibers of *Shuvuuia*, *Psittacosaurus* bristles are hyper-elongated and erect, suggesting a unique display or signaling function (Mayr et al., 2016). However, another alternate hypothesis might involve calcified, simple filaments that represent

vestigial structures as a result of secondary terrestrialization/glidelessness/flightlessness, in a manner resembling the calamus-like wing feathers on cassowaries (Prum, 2005). Thus, in a rather unusual reversal of the typical direction of evidence and interpretations for this topic of study, better resolved phylogenies and investigations pinpointing the appearance and loss of arboreality/gliding/flight using osteological data may be integral in working out feather morphology for this taxon.

4.2. False positives in paleo-immunohistochemistry

We argue that previous paleontological studies using polyclonal antibodies raised against keratin (Schweitzer et al., 1999a, 1999b; Moyer et al., 2016b, 2016b; Pan et al., 2016) have mistaken false positive results for evidence of original keratin protein preservation in fossils. Two obvious sources might yield false positive stains in *Shuvuuia* fibers and other fossilized keratinous structures: calcium phosphate or cyanoacrylate polymer.

Calcified material has been stated to yield both false negatives and positives with immunohistochemistry (Sedivy and Battistutti, 2003), while biomedical research has used cyanoacrylate nanoparticles to adsorb antibodies (Illum et al., 1983). The original study of *Shuvuuia* fibers showing positive antibody stains performed no demineralization and instead rinsed them in 100% ethanol prior to analysis (Schweitzer et al., 1999b),

which might not be expected to act as a strong enough solvent to remove cyanoacrylates through rinsing, although other consolidants applied to the fossil in the field or lab might exhibit different solubility, such as Butvar B-76. A more recent analysis resulting in positive antibody stains of *Citipati* (formerly IGM 100/979) claw sheaths (Moyer et al., 2016b), likely consolidated during collection or preparation in a similar manner to IGM 100/977, did use demineralization and revealed fibrous structures, consistent with applied organic polymers, as well as mineral grains. Antibody binding to the *Shuvuuia* fiber rim and throughout the fiber (Moyer et al., 2016a) suggests that both cyanoacrylates, or other consolidants like Butvar B-76, and calcium phosphate could be responsible for false positives.

Another issue for paleo-immunohistochemistry is that antibodies show non-specific binding to melanoidins, condensation products formed during degradation of protein and polysaccharide mixtures that can be present in fossils and sediments (Collins et al., 1992). Although we do not suspect melanoidin presence in *Shuvuuia* fibers given the limited organic content of the fibers, this could explain antibody staining of other fossils that do have organic preservation.

Since antibodies typically bind to a specific 3-dimensional epitope of the target protein, a positive result on Mesozoic fossils would suggest not only that peptides are present, but also highly preserved protein with surviving 3° or 4° structures. Higher order protein folding is unlikely to persist through deep time (Bada, 1998), therefore false positives are of

concern. In an immunological study of subfossil human skeletal material for three target proteins, antibody cross-reactivity was observed with non-human mammal bone, certain collagens, and bacterial cells (Brandt et al., 2002), calling into question the utility of immunochemistry on ancient material.

False positives from immunohistochemistry are even possible in recent, biological samples (True, 2008). The observation that "...in [a] feather treated for 10 years at 350°C, [Moyer et al.] were able to demonstrate weak positive binding of anti-feather antibodies localized to the tissues" (Moyer et al., 2016a, p. 7/18) can either be interpreted as epitope survival or the propensity for nonspecific cross-reactivity of antibodies as proteins degrade. Attempts to replicate these 350 °C conditions in a laboratory oven revealed that feathers rapidly start to smoke at this temperature and turn into a black ash (i.e., within minutes) (Supplementary Figs. S142–S143), consistent with melanoidin and other browning condensation reactions and the inferable loss of protein structure.

Ultimately, immunohistochemistry was used to support the claim that *Shuvuuia* fibers consisted of keratin protein (Schweitzer et al., 1999b; Moyer et al., 2016a). If this claim were true, then other techniques should be capable of providing multiple, independent lines of evidence that support or are consistent with a keratin protein composition. We show here that this is not the case, thereby questioning the validity the evidence evoked from immunohistochemistry.

4.3. Suggestions for future practice

Immunohistochemistry of fossils is insufficient to confirm protein preservation because of its high susceptibility to false positives. These complications are more readily diagnosed and addressed when analyzing recent, biological samples with well-established protocols and controls (True, 2008). (However, see Collins et al. (1992) for an alternative experimental procedure with antibodies, whereby antibody cross-reactivity with experimentally-produced melanoidins was observed and suggestive of Maillard-type pathways for protein-polysaccharide degradation occurring naturally in diagenesis). Other chemical tests (e.g., chromatography and mass spectrometry) can detect unique protein markers. For example, pyrolysis-gas chromatography–mass spectrometry is a sensitive, cheap method used for geologic samples, yielding a distinct suite of pyrolysates for intact or degraded proteins, particularly amides, succinimides, and diketopiperazines (Saitta et al., 2017). Additionally, liquid chromatography can be used to search for amino acids, and racemization can indicate their relative age (Bada and Schroeder 1975). Methods such as these might not be necessary, however, if the sample in question does not first show clear indication of an organic composition. Note that these methods were not used to study the *Shuvuuia* fiber since the sample failed to give fundamental chemical and structural signatures consistent with an organic, let alone proteinaceous, composition. It is also important to thoroughly extract

conserving agents from fossils prior to any analysis (Pinder et al., 2017). Our study highlights that, ideally, multiple tests should be run to produce robust claims of fossil proteins that search for organic elemental and molecular signatures, protein degradation products, and predictable amino acid racemization profiles before sequencing peptides or attempting immunohistochemical experiments.

Questionable usage of histochemical staining on fossil samples has implications beyond that of dinosaur or feather evolution. For example, Kemp (2002) used a positive result from picrosirius red (a dye used to stain collagen and amyloid in tissues) of conodont hyaline tissue as one line of evidence to conclude that collagen was originally present in the tissue, refuting homology with vertebrate enamel and leading others to claim that conodonts were not vertebrates (Turner et al., 2010). Like the antibody staining of fossil tissues, might picrosirius red staining also be susceptible to false positives in such samples, weakening this line of evidence? Further highlighting the difficulties in attempts to determine the original protein composition, or lack thereof, in a fossil tissue is the more recent proposition that conodont hyaline tissue actually contained keratin, not collagen, in early growth stages while the majority of the tissue lacked organics (Terrill et al., 2018). However, the S and organic signatures detected in the tissue through EDS and X-ray photoelectron spectroscopy by Terrill et al. (2018) are inconclusive evidence, insufficient to diagnose a keratin protein source.

5. Conclusions

Shuvuuia fibers from IGM 100/977, previously identified through immunohistochemistry as preserving keratin, are composed of calcium phosphate by virtue of their color, texture, fluorescence, elemental composition, and secondary ion mass spectra. Hardened keratin contains calcium phosphate in vivo. Thus, one hypothesis is that the fibers potentially derive from the remains of calcified feather rachi, raising the possibility of a more complex, pennaceous feather morphology in alvarezsaurids than previously thought, although simple monofilaments cannot be ruled out. Endogenous organic material or amino acid signatures could not be confirmed in the fiber. Detected organic material likely derived from applied consolidants rather than endogenous proteins based on the lack of localization of any distinct organic secondary ions to the fiber. The fiber and associated sediment matrix are covered in cyanoacrylate, likely derived from the fossil's preparation, in which cyanoacrylate and Butvar B-76 were applied. Cyanoacrylates and other substances, potentially including calcium phosphate, can accumulate antibodies, likely explaining previous reports of keratin preservation in these fibers as false positives. As suggested by our study, immunohistochemistry on fossils is likely inappropriate for studying ancient, putative proteins without independent, corroborative evidence, and even then, the possibility of contamination in corroborating methods should be controlled for.

Acknowledgements

Thanks to Amy Davidson for providing details of the preparation of IGM 100/977, Matthew J. Collins, Christian Foth, Jasmina Wiemann and Michael Buckley for helpful comments, and John Cunningham for assistance in producing polished sections. SOR acknowledges funding from the Marie Skłodowska-Curie Actions Programs and the Irish Research Council (ELEVATE Career Development Fellowship ELEVATEPD/2014/47). Work at MIT was supported by the NASA Astrobiology Institute (NNA13AA90A). MP and TGK were supported by the Dr. Stephen S. F. Hui Trust Fund (201403173007). MP was also supported by the Research Grant Council of Hong Kong's General Research Fund (17103315) and the Faculty of Science of the University of Hong Kong. MAN acknowledges support of AMNH. Funding sources had no involvement in study design, collection, analysis, and interpretation of data, writing of the report, and the decision to submit the article for publication. We acknowledge the editor and helpful reviews of three anonymous reviewers. Written in memory of James O'Shea.

Appendix A. Supplementary material

Supplementary data associated with this article can be found, in the online version at xxxxxx. These include a supplementary PDF file along with four .XLSX/.CSV and four .TXT raw data files.

Associate Editor–Klaas Nierop

References

Armstrong, W.G., Halstead, L.B., Reed, F.B., Wood, L., 1983. Fossil proteins in vertebrate calcified tissues. Philosophical Transactions of the Royal Society of London B: Biological Sciences 301, 301–343.

Asara, J.M., Schweitzer, M.H., Freimark, L.M., Phillips, M., Cantley, L.C., 2007. Protein sequences from mastodon and *Tyrannosaurus rex* revealed by mass spectrometry. Science 316, 280–285.

Bada, J.L., 1998. Biogeochemistry of organic nitrogen compounds. In: Stankiewicz, B.A., van Bergen, P.F. (Eds.), Nitrogen-Containing Macromolecules in the Bio- and Geosphere. Oxford University Press, Oxford, pp. 64–73.

Bada, J.L., Schroeder, R.A., 1975. Amino acid racemization reactions and their geochemical implications. Naturwissenschaften 62, 71–79.

Baggott, D.G., Bunch, K.J., Gill, K.R., 1988. Variations in some inorganic components and physical properties of claw keratin associated with claw disease in the British Friesian cow. British Veterinary Journal 144, 534–542.

Bell, P.R., 2012. Standardized terminology and potential taxonomic utility for hadrosaurid skin impressions: a case study for *Saurolophus* from Canada and Mongolia. PLoS One 7, e31295.

Bell, P.R., Campione, N.E., Persons, W.S., Currie, P.J., Larson, P.L., Tanke, D.H., Bakker, R.T., 2017. Tyrannosauroid integument reveals

conflicting patterns of gigantism and feather evolution. Biology Letters 13, 20170092.

Benton, M.J., Zhonghe, Z., Orr, P.J., Fucheng, Z., Kearns, S.L., 2008. The remarkable fossils from the Early Cretaceous Jehol Biota of China and how they have changed our knowledge of Mesozoic life. Proceedings of the Geologists' Association 119, 209–228.

Bergmann, U., Morton, R.W., Manning, P.L., Sellers, W.I., Farrar, S., Huntley, K.G., Wogelius, R.A., Larson, P., 2010. *Archaeopteryx* feathers and bone chemistry fully revealed via synchrotron imaging. Proceedings of the National Academy of Sciences of the United States of America 107, 9060–9065.

Bertazzo, S., Maidment, S.C., Kallepitis, C., Fearn, S., Stevens, M.M., Xie, H.N., 2015. Fibres and cellular structures preserved in 75-million-year-old dinosaur specimens. Nature Communications 6, 7352.

Blakey, P.R., Lockwood, P., 1968. The environment of calcified components in keratins. Calcified Tissue International 2, 361–369.

Blakey, P.R., Earland, C., Stell, J.G.P., 1963. Calcification of keratin. Nature 198, 481–481.

Bonser, R.H., 1996. Comparative mechanics of bill, claw and feather keratin in the Common Starling *Sturnus vulgaris*. Journal of Avian Biology 27, 175–177.

Brandt, E., Wiechmann, I., Grupe, G., 2002. How reliable are immunological tools for the detection of ancient proteins in fossil bones? International Journal of Osteoarchaeology 12, 307–316.

Briggs, D.E., 2003. The role of decay and mineralization in the preservation of soft-bodied fossils. Annual Review of Earth and Planetary Sciences 31, 275–301.

Briggs, D.E., Summons, R.E., 2014. Ancient biomolecules: their origins, fossilization, and role in revealing the history of life. BioEssays 36, 482–490.

Briggs, D.E., Wilby, P.R., 1996. The role of the calcium carbonate-calcium phosphate switch in the mineralization of soft-bodied fossils. Journal of the Geological Society 153, 665–668.

Briggs, D.E.G., Kear, A.J., Martill, D.M., Wilby, P.R., 1993. Phosphatization of soft-tissue in experiments and fossils. Journal of the Geological Society 150, 1035–1038.

Brown, C.M., Henderson, D.M., Vinther, J., Fletcher, I., Sistiaga, A., Herrera, J., Summons, R.E., 2017. An exceptionally preserved three-dimensional armored dinosaur reveals insights into coloration and cretaceous predator-prey dynamics. Current Biology 27, 2514–2521.

Cau, A., Brougham, T., Naish, D., 2015. The phylogenetic affinities of the bizarre Late Cretaceous Romanian theropod *Balaur bondoc* (Dinosauria, Maniraptora): dromaeosaurid or flightless bird? PeerJ 3, e1032.

Christiansen, N.A., Tschopp, E., 2010. Exceptional stegosaur integument impressions from the Upper Jurassic Morrison Formation of Wyoming. Swiss Journal of Geosciences 103, 163–171.

Collins, M.J., Westbroek, P., Muyzer, G., de Leeuw, J.W., 1992. Experimental evidence for condensation reactions between sugars and proteins in carbonate skeletons. Geochimica et Cosmochimica Acta 56, 1539–1544.

Collins, M.J., Walton, D., Curry, G.B., Riley, M.S., Von Wallmenich, T.N., Savage, N.M., Muyzer, G., Westbroek, P., 2003. Long-term trends in the survival of immunological epitopes entombed in fossil brachiopod skeletons. Organic Geochemistry 34, 89–96.

Curry, G.B., Cusack, M., Walton, D., Endo, K., Clegg, H., Abbott, G., Armstrong, H., 1991. Biogeochemistry of brachiopod intracrystalline molecules. Proceedings of the Royal Society B: Biological Sciences 333, 359–366.

Davies, A., 1970. Micromorphology of feathers using the scanning electron microscope. Journal of the Forensic Science Society 10, 165–174.

De Jong, E.W., Westbroek, P, Westbroek, J.F., Bruning, J.W., 1974. Preservation of antigenic properties of macromolecules over 70 Myr. Nature 252, 63–64.

Demarchi, B., Hall, S., Roncal-Herrero, T., Freeman, C.L., Woolley, J., Crisp, M.K., Wilson, J., Fotakis, A., Fischer, R., Kessler, B.M., Jersie-Christensen, R.R., 2016. Protein sequences bound to mineral surfaces

persist into deep time. Elife 5, e17092.

Fürsich, F.T., Sha, J., Jiang, B., Pan, Y., 2007. High resolution palaeoecological and taphonomic analysis of Early Cretaceous lake biota, western Liaoning (NE-China). Palaeogeography, Palaeoclimatology, Palaeoecology 253, 434–457.

Gioncada, A., Collareta, A., Gariboldi, K., Lambert, O., Di Celma, C., Bonaccorsi, E., Urbina, M., Bianucci, G., 2016. Inside baleen: exceptional microstructure preservation in a late Miocene whale skeleton from Peru. Geology 44, 839–842.

Goddard, D.R., Michaelis, L., 1934. A study of keratin. Journal of Biological Chemistry 106, 604–614.

Greenwold, M.J., Sawyer, R.H., 2011. Linking the molecular evolution of avian beta (β) keratins to the evolution of feathers. Journal of Experimental Zoology Part B: Molecular and Developmental Evolution 316, 609–616.

Gurley, L.R., Valdez, J.G., Spall, W.D., Smith, B.F., Gillette, D.D., 1991. Proteins in the fossil bone of the dinosaur, *Seismosaurus*. Journal of Protein Chemistry 10, 75–90.

Hedberg, Y., Killian, M.S., Blomberg, E., Virtanen, S., Schmuki, P., Odnevall Wallinder, I., 2012. Interaction of bovine serum albumin and lysozyme with stainless steel studied by time of flight secondary ion mass spectrometry and x-ray photoelectron spectroscopy. Langmuir 28, 16306–16317.

Illum, L., Jones, P.D.E., Kreuter, J., Baldwin, R.W., Davis, S.S., 1983. Adsorption of monoclonal antibodies to polyhexylcyanoacrylate nanoparticles and subsequent immunospecific binding to tumour cells in vitro. International Journal of Pharmaceutics 17, 65–76.

Kaye, T.G., Falk, A.R., Pittman, M., Sereno, P.C., Martin, L.D., Burnham, D.A., Gong, E., Xu, X., Wang, Y., 2015. Laser-stimulated fluorescence in paleontology. PloS One 10, e0125923.

Kemp, A., 2002. Amino acid residues in conodont elements. Journal of Paleontology 76, 518–528.

Kriausakul, N., Mitterer, R.M., 1978. Isoleucine epimerization in peptides and proteins: Kinetic factors and application to fossil proteins. Science 201, 1011–1014.

Laver, W.G., Air, G.M., Webster, R.G., Smith-Gill, S.J., 1990. Epitopes on protein antigens: misconceptions and realities. Cell 61, 553–556.

Lowenstein, J.M., 1985. Molecular approaches to the identification of species: immunological analysis of proteins from living or fossil organisms can be used to identify unrecognizable species and to obtain new information on taxonomic relationships and dates of evolutionary divergence. American Scientist 73, 541–547.

Lucas, A.M., Stettenheim, P.R., 1972. Avian Anatomy Integument. US Government Printing Office, Washington, DC.

Martin, L.D., Zhou, Z.H., Hou, L., Feduccia, A., 1998. *Confuciusornis sanctus* compared to *Archaeopteryx lithographica*. Naturwissenschaften 85, 286–289.

Mayr, G., Pittman, M., Saitta, E., Kaye, T.G., Vinther, J., 2016. Structure and homology of *Psittacosaurus* tail bristles. Palaeontology 59, 793–802.

Mitterer, R.M., 1993. The diagenesis of proteins and amino acids in fossil shells. In: Engel, M.H., Macko, S.A. (Eds.), Organic Geochemistry. Springer, Boston, pp. 739–753.

Moyer, A.E., Zheng, W., Schweitzer, M.H., 2016a. Keratin durability has implications for the fossil record: Results from a 10 year feather degradation experiment. PloS One 11, e0157699.

Moyer, A.E., Zheng, W., Schweitzer, M.H., 2016b. Microscopic and immunohistochemical analyses of the claw of the nesting dinosaur, *Citipati osmolskae*. Proceedings of the Royal Society B: Biological Sciences 283, 20161997.

Murphy, N.L., Trexler, D., Thompson, M., 2006. "Leonardo," a mummified *Brachylophosaurus* from the Judith River Formation. In: Carpenter, K. (Ed.), Horns and Beaks: Ceratopsian and Ornithopod Dinosaurs. Indiana University Press, Bloomington, pp. 117–133.

Norell, M.A., Xu, X., 2005. Feathered dinosaurs. Annual Review of Earth and Planetary Sciences 33, 277–299.

Orlando L, Ginolhac, A., Zhang, G., Froese, D., Albrechtsen, A., Stiller, M.,

Schubert, M., Cappellini, E., Petersen, B., Moltke, I., Johnson, P.L.F., Fumagalli, M., Vilstrup, J.T., Raghavan, M., Korneliussen, T., Malaspinas, A.S., Vogt, J., Szklarczyk, D., Kelstrup, C.D., Vinther, J., Dolocan, A., Stenderup, J., Velazquez, A.M.V., Cahill, J., Rasmussen, M., Wang, X., Min, J., Zazula, G.D., Seguin-Orlando, A., Mortensen, C., Magnussen, K., Thompson, J.F., Weinstock, J., Gregersen, K., Røed, K.H., Eisenmann, V., Rubin, C.J., Miller, D.C., Antczak, D.F., Bertelsen, M.F., Brunak, S., Alrasheid, K.A.S., Ryder, O., Andersson, L., Mundy, J., Krogh, A., Gilbert, M.T.P., Kjær, K., Sicheritz-Ponten, T., Jensen, L.J., Olsen, J.V., Hofreiter, M., Nielsen, R., Shapiro, B., Wang, J., Willerslev, E., 2013. Recalibrating *Equus* evolution using the genome sequence of an early Middle Pleistocene horse. Nature 499, 74–78.

Pan, Y., Zheng, W., Moyer, A.E., O'Connor, J.K., Wang, M., Zheng, X., Wang, X., Schroeter, E.R., Zhou, Z., Schweitzer, M.H., 2016. Molecular evidence of keratin and melanosomes in feathers of the Early Cretaceous bird *Eoconfuciusornis*. Proceedings of the National Academy of Sciences of the United States of America 113, E7900–E7907.

Parry, L.A., Wilson, P., Sykes, D., Edgecombe, G.D., Vinther, J., 2015. A new fireworm (Amphinomidae) from the Cretaceous of Lebanon identified from three-dimensionally preserved myoanatomy. BMC Evolutionary Biology, 15, 256.

Parry, L.A., Smithwick, F., Nordén, K.K., Saitta, E.T., Lozano-Fernandez, J., Tanner, A.R., Caron, J.B., Edgecombe, G.D., Briggs, D.E., Vinther, J., 2018. Soft-bodied fossils are not simply rotten carcasses–toward a holistic understanding of exceptional fossil preservation. BioEssays 40, 1700167.

Pautard, F.G.E., 1963. Mineralization of keratin and its comparison with the enamel matrix. Nature 19, 531–535.

Pautard, F.G.E., 1964. Calcification of keratin. In: Rook, A., Champion, R.H. (Eds.), Progress in the Biological Sciences in Relation to Dermatology–2. Cambridge University Press, Cambridge, pp. 227–240.

Pautard, F.G.E., 1970. The mineral phase of calcified cartilage, bone and baleen. Calcified Tissue Research 4, 34–36.

Pinder, A.P., Panter, I., Abbott, G.D., Keely, B.J., 2017. Deterioration of the Hanson Logboat: Chemical and imaging assessment with removal of polyethylene glycol conserving agent. Scientific Reports 7, 13697.

Prum, R.O., 2005. Evolution of the morphological innovations of feathers. Journal of Experimental Zoology Part B: Molecular and Developmental Evolution 304, 570–579.

Rybczynski, N., Gosse, J.C., Harington, C.R., Wogelius, R.A., Hidy, A.J., Buckley, M., 2013. Mid-Pliocene warm-period deposits in the High Arctic yield insight into camel evolution. Nature Communications 4, 1550.

Saitta, E.T., Rogers, C, Brooker, R.A., Abbott, G.D., Kumar, S., O'Reilly, S.S., Donohoe, P., Dutta, S., Summons, R.E., Vinther, J., 2017. Low fossilization potential of keratin protein revealed by experimental taphonomy. Palaeontology 60, 547–556.

Schweitzer, M.H., Watt, J.A., Avci, R., Forster, C.A., Krause, D.W., Knapp, L., Rogers, R.R., Beech, I., Marshall, M. 1999a. Keratin immunoreactivity in the Late Cretaceous bird *Rahonavis ostromi*. Journal of Vertedbrate Paleontology 19, 712–722.

Schweitzer, M.H., Watt, J.A., Avci, R., Knapp, L., Chiappe, L., Norell, M., Marshall, M. 1999b. Beta-keratin specific immunological reactivity in feather-like structures of the Cretaceous Alvarezsaurid, *Shuvuuia deserti*. Journal of Experimental Zoology Part B: Molecular and Developmental Evolution 285, 146–157.

Schweitzer, M.H., Wittmeyer, J.L., Horner, J.R., Toporski, J.K., 2005. Soft-tissue vessels and cellular preservation in *Tyrannosaurus rex*. Science 307, 1952–1955.

Schweitzer, M.H., Suo, Z., Avci, R., Asara, J.M., Allen, M.A., Arce, F.T., Horner, J.R., 2007. Analyses of soft tissue from *Tyrannosaurus rex* suggest the presence of protein. Science 316, 277–280.

Schweitzer, M.H., Zheng, W., Organ, C.L., Avci, R., Suo, Z., Freimark, L.M., Lebleu, V.S., Duncan, M.B., Vander Heiden, M.G., Neveu, J.M., Lane, W.S., 2009. Biomolecular characterization and protein sequences of the Campanian hadrosaur *B. canadensis*. Science 324, 626–631.

Schwieters, J., Cramer, H.-G., Heller, T., Jürgens, U., Niehuis, E., Zehnpfenning, J., Benninghoven, A., 1991. High mass resolution surface imaging with a time-of-flight secondary ion mass spectroscopy scanning microprobe. Journal of Vacuum Science and Technology A 9, 2864–2871.

Sedivy, R., Battistutti, W.B., 2003. Nanobacteria promote crystallization of psammoma bodies in ovarian cancer. Apmis 111, 951–954.

Smithwick, F.M., Mayr, G., Saitta, E.T., Benton, M.J., Vinther, J., 2017. On the purported presence of fossilized collagen fibres in an ichthyosaur and a theropod dinosaur. Palaeontology 60, 409–422.

Szewciw, L.J., De Kerckhove, D.G., Grime, G.W., Fudge, D.S., 2010. Calcification provides mechanical reinforcement to whale baleen α-keratin. Proceedings of the Royal Society B: Biological Sciences 277, 2597–2605.

Terrill, D.F., Henderson, C.M., Anderson, J.S., 2018. New applications of spectroscopy techniques reveal phylogenetically significant soft tissue residue in Paleozoic conodonts. Journal of Analytical Atomic Spectrometry 33, 992–1002.

True, L.D., 2008. Quality control in molecular immunohistochemistry. Histochemistry and Cell Biology 130, 473–480.

Turner, S., Burrow, C.J., Schultze, H.P., Blieck, A., Reif, W.E., Rexroad, C.B., Bultynck, P., Nowlan, G.S., 2010. False teeth: conodont-

vertebrate phylogenetic relationships revisited. Geodiversitas 32, 545–594.

Vinther, J., 2015. A guide to the field of palaeo colour. BioEssays 37, 643–656.

Vinther, J., Nicholls, R., Lautenschlager, S., Pittman, M., Kaye, T.G., Rayfield, E., Mayr, G., Cuthill, I.C., 2016. 3D camouflage in an ornithischian dinosaur. Current Biology 26, 2456–2462.

Walton, D., 1998. Degradation of intracrystalline proteins and amino acids in fossil brachiopods. Organic Geochemistry 28, 389–410.

Wang, X., Pittman, M., Zheng, X., Kaye, T.G., Falk, A.R., Hartman, S.A., Xu, X., 2017. Basal paravian functional anatomy illuminated by high-detail body outline. Nature Communications 8, 14576.

Xu, X., Wang, K., Zhang, K., Ma, Q., Xing, L., Sullivan, C., Hu, D., Cheng, S., Wang, S., 2012. A gigantic feathered dinosaur from the Lower Cretaceous of China. Nature 484, 92–95.

Xu, X., Zhou, Z., Dudley, R., Mackem, S., Chuong, C.M., Erickson, G.M., Varricchio, D.J., 2014. An integrative approach to understanding bird origins. Science 346, 1253293.

Figure legends

Fig. 1. *Shuvuuia* (IGM 100/977) fiber analyzed. (A–D) Untreated fiber. (A–C) Light micrographs. (A) Whole fiber. (B) Basal end. (C) Apical region. (D) LSF image of basal portion showing unique fluorescence in color and

intensity relative to the matrix. (E) Scanning electron image of FIB trench in fiber.

Fig. 2. Resin-embedded polished sample TOF-SIMS. Fiber in center. Fragment ions associated with (B–F) fiber, (G–O) sediment matrix, (P–R) applied residues, and (S–MM) potential amino acids or their derivatives, including peaks identified by Hedberg et al. (2012). (B) Sum of Ca^+, total CaO_X^+, and total $CaPO_X^+$. (C) Sum of $CaOH^+$, Ca_2O^+, and $Ca_2O_2H^+$. (D) Sum of $CaPO_2^+$, $CaPO_3^+$, $Ca_2PO_3^+$, $Ca_2PO_4^+$, $Ca_3PO_4^+$, and $Ca_3PO_5^+$. (F) Sum of PO_2^- and PO_3^-. (N) Sum of SiO_2^-, SiO_3^-, $HSiO_3^-$, $Si_2O_4^-$, $Si_2O_4H^-$, and $Si_2O_5H^-$. (P) Sum of CH_3O^+, m/z = 135, and m/z = 191. (Q) Sum of m/z = –211 and m/z = –283. (R) Sum of $C_5H_6NO_2^-$ and $C_{10}H_{12}N_2O_4^-$. (KK) Sum of images (S) to (BB) and (DD) to (JJ) inclusive. (LL) Sum of S^-, HS^-, SO_2^-, and SO_3^-.

Fig. 3. EDS of resin-embedded polished sample. Fiber in center. Significant peaks of region analysis of fiber (A) labelled in spectrum (J).

Figure 1

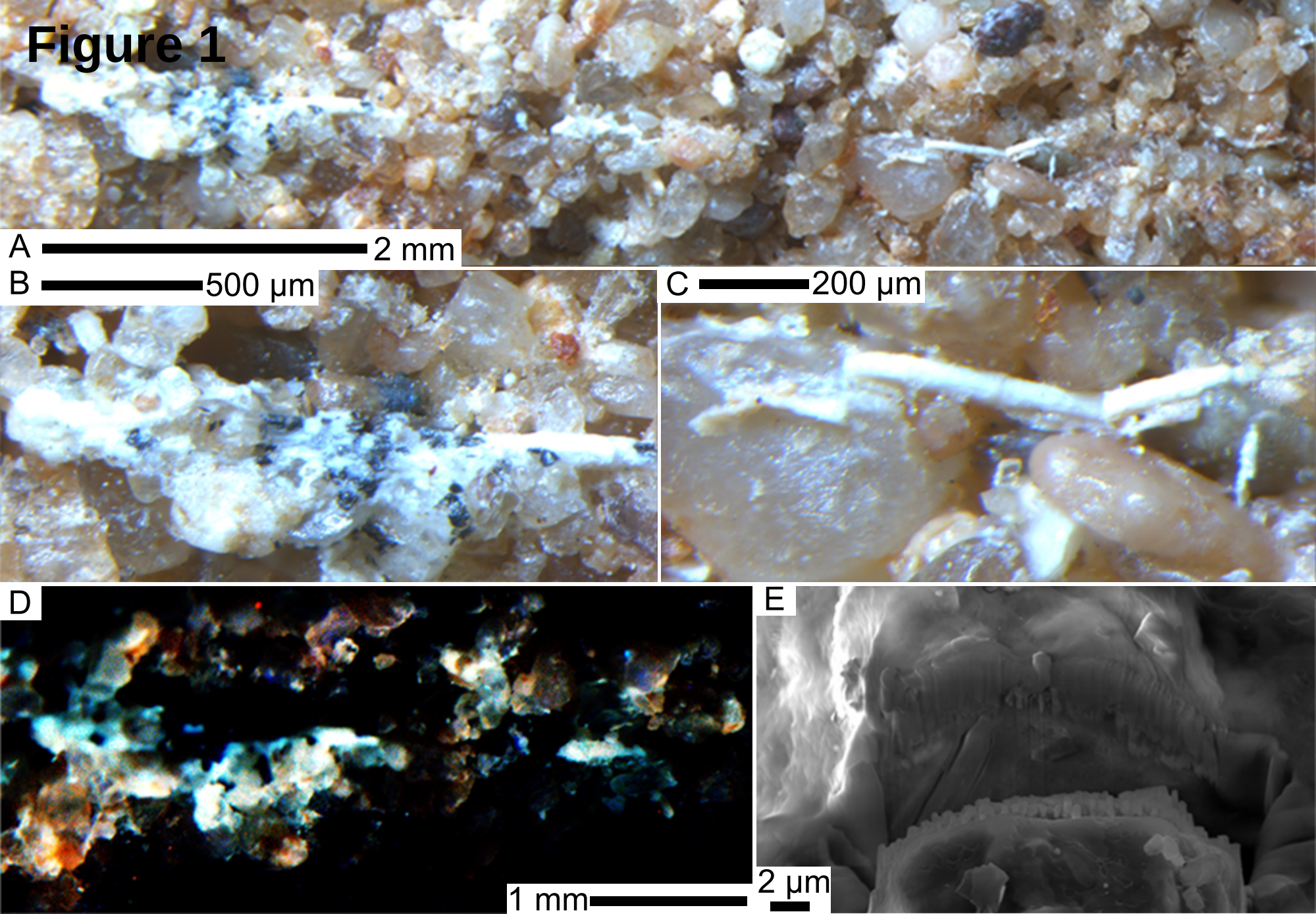

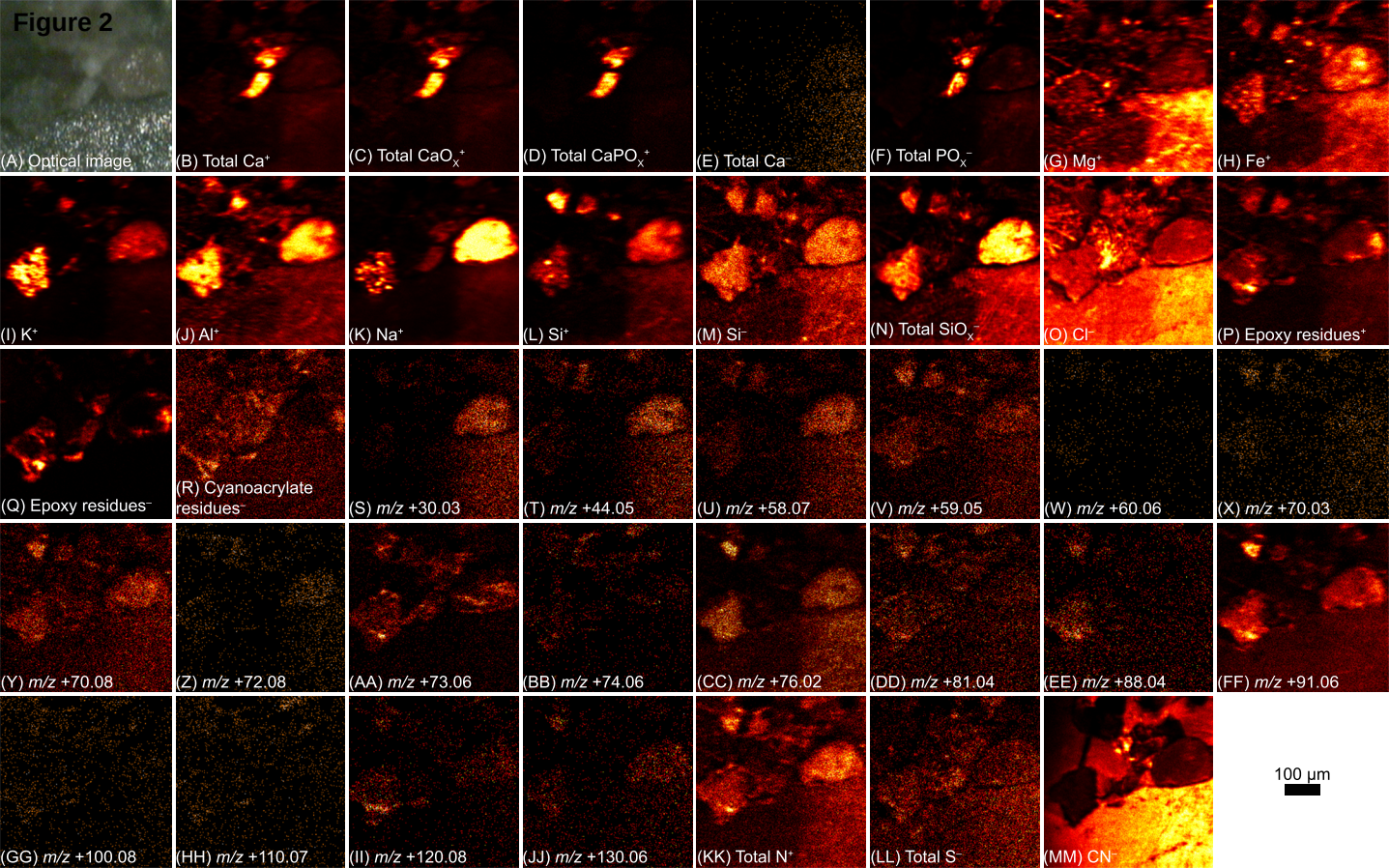
Figure 2
(A) Optical image
(B) Total Ca+
(C) Total CaOx+
(D) Total CaPOx+
(E) Total Ca−
(F) Total POx−
(G) Mg+
(H) Fe+
(I) K+
(J) Al+
(K) Na+
(L) Si+
(M) Si−
(N) Total SiOx−
(O) Cl−
(P) Epoxy residues+
(Q) Epoxy residues−
(R) Cyanoacrylate residues−
(S) m/z +30.03
(T) m/z +44.05
(U) m/z +58.07
(V) m/z +59.05
(W) m/z +60.06
(X) m/z +70.03
(Y) m/z +70.08
(Z) m/z +72.08
(AA) m/z +73.06
(BB) m/z +74.06
(CC) m/z +76.02
(DD) m/z +81.04
(EE) m/z +88.04
(FF) m/z +91.06
(GG) m/z +100.08
(HH) m/z +110.07
(II) m/z +120.08
(JJ) m/z +130.06
(KK) Total N+
(LL) Total S−
(MM) CN−
100 µm

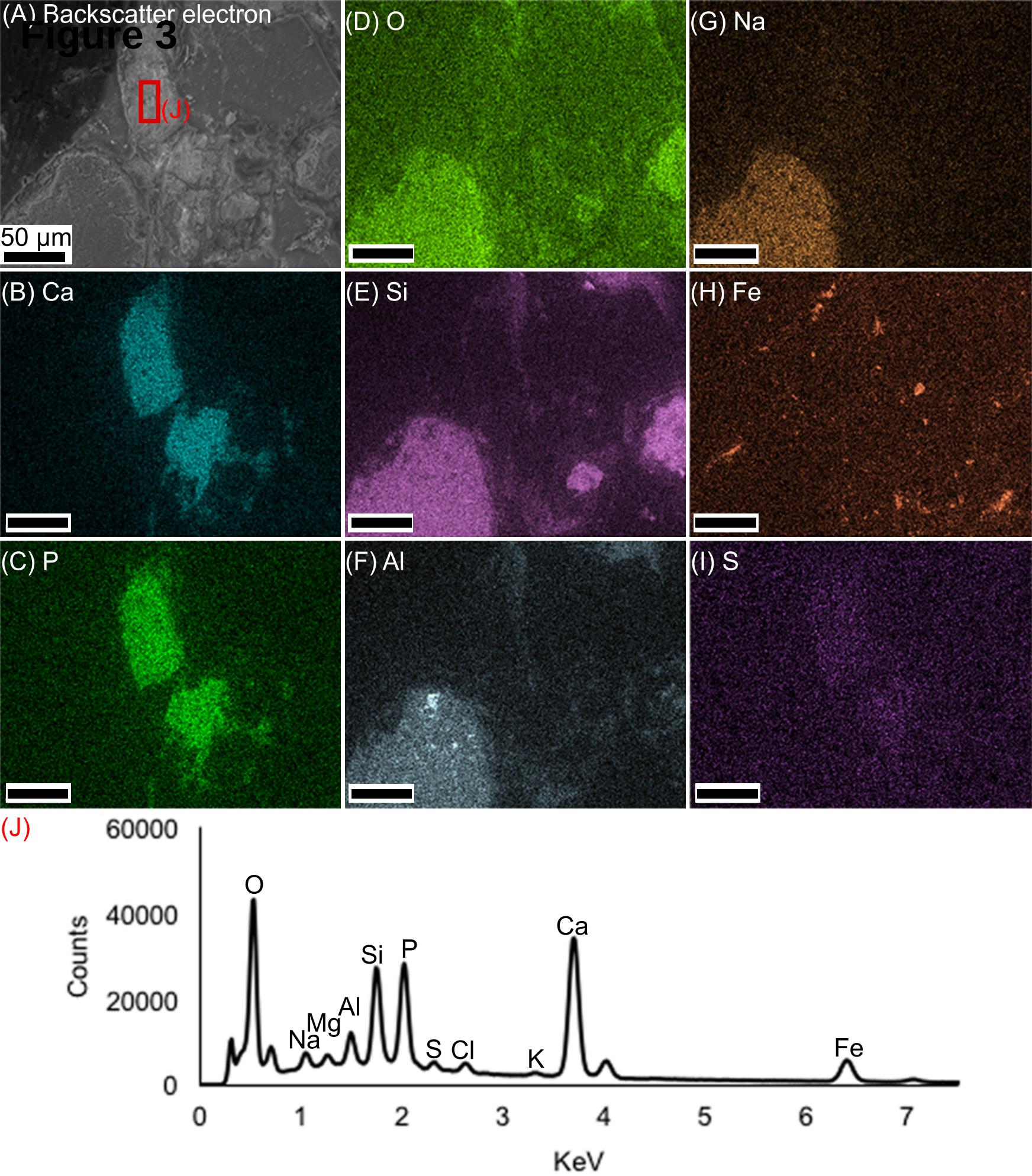
(A) Backscatter electron
Figure 3
(J)
50 µm
(D) O
(G) Na
(B) Ca
(E) Si
(H) Fe
(C) P
(F) Al
(I) S
(J)
60000
40000
20000
0
Counts
O
Na
Mg
Al
Si
P
S
Cl
K
Ca
Fe
0
1
2
3
4
5
6
7
KeV

Highlights

- Immunohistochemistry has been used to claim fossil protein preservation.
- Reanalysis of a fossil feather reveals that it is inorganic, not proteinaceous.
- The fossil feather was also covered in cyanoacrylate consolidant.
- Antibody cross-reactivity might lead to false positive results in fossils.
- Claims for ancient proteins require multiple lines of corroborating evidence.